

Article

Investigation of the Inhibition Potential of New Oxindole Derivatives and Assessment of Their Usefulness for Targeted Therapy

Przemysław Czelen[†]

Department of Physical Chemistry, Faculty of Pharmacy, Collegium Medicum, Nicolaus Copernicus University, Kurpińskiego 5, 85-096 Bydgoszcz, Poland; przemekcz@cm.umk.pl

Received: 29 June 2019; Accepted: 27 July 2019; Published: 1 August 2019



Abstract: Oxindole derivatives are a large group of compounds that can play the role of Adenosine triphosphate (ATP) competitive inhibitors. The possibility of modification of such compounds by addition of active groups to both cyclic systems of oxindole allows the obtaining of derivatives showing significant affinity toward cyclin-dependent kinase (CDK) proteins. Overexpression of that enzyme is observed in the case of most cancers. The discovery of new efficient inhibitors, which could be used in the development of targeted therapies, is one of the current goals setting trends in recent research. In this research, an oxindole molecular core was used, which was modified by the addition of different substituents to both side chains. The realized procedure allowed the creation of a set of oxindole derivatives characterized by binding affinity values and molecular descriptors evaluated during docking procedures and QSAR calculations. The most promising structures characterized by best sets of parameters were used during the molecular dynamics stage. The analysis of structural and energetic properties of systems obtained during this stage of computation gives an indication of inhibitors creating the most stable complexes, characterized by the highest affinity. During this stage, two structures were selected, where affinity towards potential nanocarriers was evaluated. Realized calculations confirmed a significant role of stacking interactions in the stabilization of ligand complexes with fullerene molecules. Obtained data indicates that complexes of oxindole derivatives and considered nanocarriers exhibit significant potential in the creation of immobilized drugs, and can be used in the development of targeted therapies.

Keywords: CDK-2; oxindoles; docking; molecular dynamics; MMPBSA; inhibition; C₆₀ fullerene derivatives

1. Introduction

The process of cell proliferation is crucial for all living organisms. The regulation of the cell cycle is strictly related to the action of a set of SER/THR kinases classified as cyclin-dependent kinases (CDKs). All these proteins, after complexation with activate factors called cyclins, play the role of regulation of activity of other proteins involved in transcription and replication processes [1–3]. Among all CDK proteins the most crucial role in progression of the cell cycle is assigned to CDK2. Overexpression of that enzyme is often observed in the case of most cancers [2,4–7]. The search for the ATP competitive inhibitors of CDK2 is important in the context of creation of anticancer therapies. The example of a natural product exhibiting such properties is indirubin [8,9] the anticancer properties of this compound were widely known and used in traditional Chinese medicine. The chemical structure of the indirubin molecule consists of two conjugated oxindoles. The derivatives and analogs of indirubine represent a large group of new CDK2 inhibitors [10–14]. The oxindole core was repeatedly the basis of the creation of ATP competitive inhibitors. Luk et al showed that the addition of active groups to both cyclic systems of oxindole allows the obtaining of derivatives showing significant affinity toward the

CDK2 active site, which can also exhibit selective potential in the context of interactions with proteins from the CDK family [15,16]. The CDK2 inhibitors analyzed in earlier works [17,18] confirm that the oxindole core with a carbonyl group substituted in C5 position exhibits high affinity toward the CDK2 active site. The presence of hydrogen-bond donors and acceptors in this structure provides strong anchorage in the space of the active site through characteristic interaction with Glu 81, Leu 83, and Lys 33 [17,18] (see Figure 1). In this work, it was proposed to use such a structure as the basic core of new oxindole derivatives created by the addition of a set of different active groups exhibiting diverse binding properties (see Figure 2). The screening of obtained structures, including binding affinity and molecular properties, allows for the prediction of new ATP competitive inhibitors well suited to the structural and binding properties of the CDK2 active site. An important aspect of drug development is also the finding of effective delivery methods. One commonly used technique in the creation of targeted therapies is immobilization of drugs with the use of different types of carriers [19–21], which ensures their direct delivery and release to the appropriate biological target. The use of such a method has other potential related effects, e.g., decreasing drug toxicity [22,23], and increasing its bioavailability and elongation of pharmacological action [24,25]. One of the most commonly used nanomolecules employed for such an aim is C₆₀ fullerene and its derivatives [23,26–29]. Such a molecule exhibits high affinity towards biologically active molecules containing aromatic systems. This popular fullerene exhibits biological activity towards cells [27], its characteristic chemical structure enables good permeation through cell membrane [30,31], and small concentrations of this compound are nontoxic for living organisms. The investigation of oxindole derivative binding potential relative to C₆₀ and its derivatives allows evaluation of the possibilities of their use in the creation of targeted therapies.

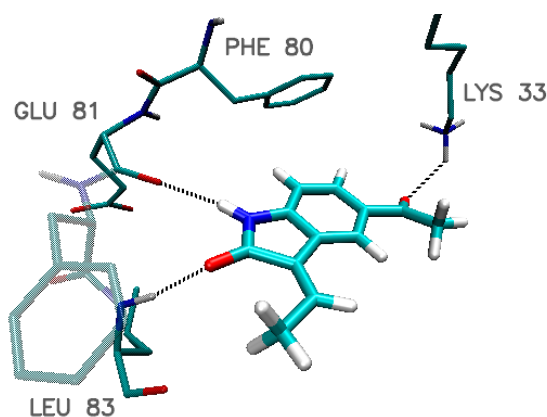


Figure 1. The hydrogen bonds and stacking interactions characteristic for oxindole core with amino acids from CDK2 active site.

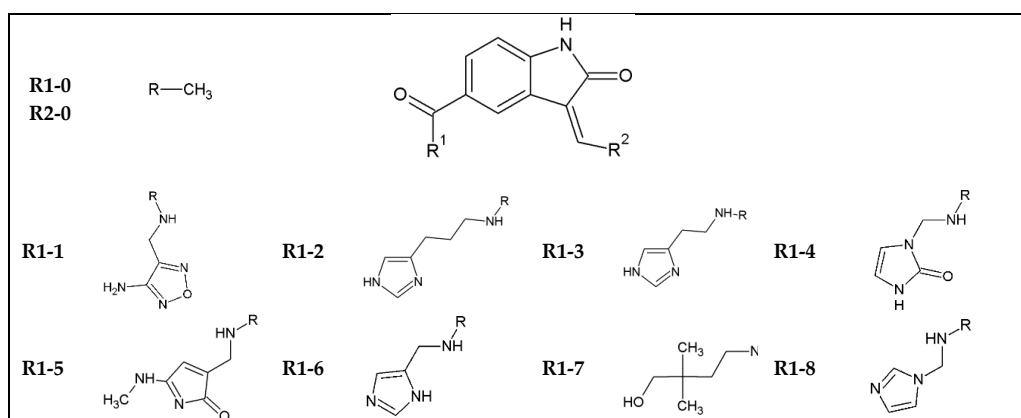


Figure 2. Cont.

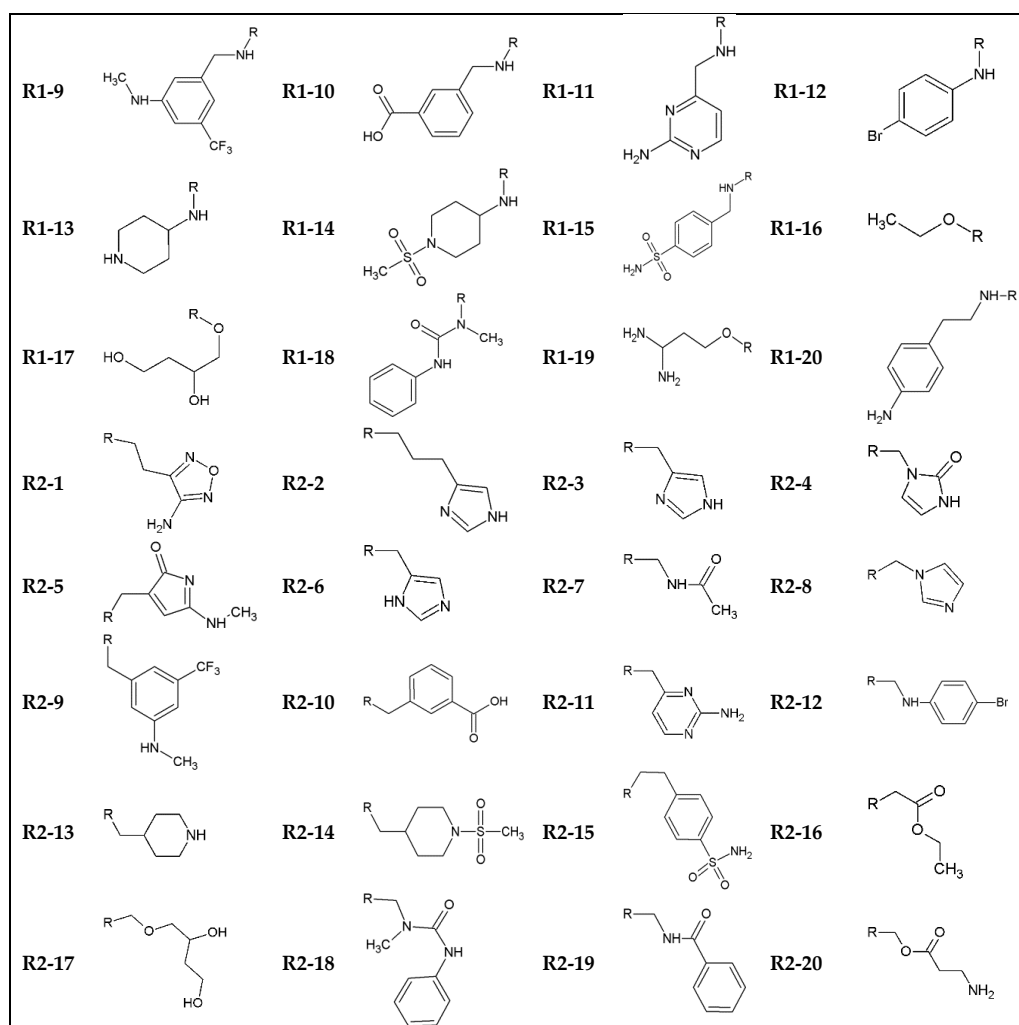


Figure 2. The graphic representation of oxindole core and active groups used during the creation of ligands.

2. Methods

Ligand structures were created by the addition of 20 different active groups to both side chains of the oxindole core. In the first step, only one side chain was replaced by an active group, while the second was represented by a methyl group. In this way, such active groups were determined, which increase binding affinity of ligand towards the CDK2 active site with the preservation of interactions characteristic for indoline derivatives identified in previous works [17,18]. A total of 84 different indoline derivatives were created with the use of seven active groups in R1 position and 14 in R2. The designation of the structures created in this procedure contains the prefix (Indol_) and the numbers of the bases used in positions R1 and R2. All considered structures were optimized during computations with the use of TURBOMOL at COSMO-BP-tzvpd-fine level of theory [32]. The toxicity of obtained molecules was simulated using a combination of the 3D/4D QSAR (Quantitative structure–activity relationship) BiS/MC and CoCon algorithms [33,34] with the use of the Chemosophia application [35]. The octanol–water partition coefficient (LogP) was determined with use of the COSMOTHERM application [36]. All docking procedures were realized with the use of AutoDockVina [37]. The C₆₀ structure and cyclin-dependent kinase 2 (CDK2-PDB ID 1E9H) were downloaded from Brookhaven Protein Database PDB, while C₆₀ functionalized derivatives were obtained from PubChem database [38]. All calculations were realized with the use of chemical structures of ligands, protein, and nanocarriers containing only polar hydrogen atoms. All initial steps were realized with the use of the AutoDock

Tolls package [39]. To confirm the location of the active site and to exclude the presence of competitive interactions on the surface of the protein, blind docking was performed [40,41]. The size of the grid box was $72 \times 84 \times 66 \text{ \AA}$ and covered the entire surface of the protein. The realized preliminary calculations confirmed the localization of the active site and the dimensions of the grid box were fitted to the size of active site of CDK2 enzyme ($16 \times 14 \times 22 \text{ \AA}$). In the case of all nanoparticles, the grid box dimensions were established equal to $26 \times 26 \times 26 \text{ \AA}$. During the molecular dynamics procedure, there were structures of complexes created by CDK-2 protein with chosen ligand molecules. Ligand structures were characterized using generalized amber force-field parameters. In the case of the CDK-2 protein, the ff14SB Force Field [42] was used and the atomic charges were calculated according to the Merz–Kollmann scheme via the RESP (Restrained electrostatic potential atomic partial charges) procedure at HF/6-31G* level [43]. Each system was neutralized with the use of three chloride anions and immersed in a periodic box ($79 \times 86 \times 71 \text{ \AA}$) consisting of 14,809 TIP3P water molecules. Considered systems were heated to 300K by 100 ps of initial MD simulation, while the temperature was controlled by Langevin thermostat [44]. The minimization and heating of systems was realized with constant-volume periodic boundaries (NTB = 1), while the proper production of molecular dynamics was realized with constant pressure (NTB = 2). The periodic boundary conditions and SHAKE algorithm were applied for 80 ns of molecular dynamic simulation; the first 20 ns of simulation time was used as equilibration interval, and the next 60 ns of the trajectory were used in the analysis of the interaction between the considered subunits. Structural analysis was performed with use of the VMD package [45]. The energetic characteristic of interaction between the ligand and the active site was obtained with the use of Molecular Mechanic/Poisson–Boltzmann Surface Area (MMPBSA) method [46]. In all molecular dynamics simulations, the AMBER 14 package was used [47]. During analysis of interactions in the active site, the hydrogen bonds were defined by the following criteria: the distance between donor (D) and acceptor (A) $< 3.5 \text{ \AA}$, angle D–H–A $> 90^\circ$, and distance H–A $< 3 \text{ \AA}$.

3. Results and Discussion

The structures of ligand molecules obtained by the addition of a single functional group to the oxindole core of the molecule were docked to the CDK2 active site. Each obtained complex preserved characteristic interactions between the oxindole core and the CDK2 active site, namely with LEU 83, GLU 81, and LYS 33. The binding affinities of considered structures toward protein are presented in Table 1. The modifications applied to the R1 position in 16 cases increased the binding affinity of the ligand toward the CDK2 active site. The highest observed increase of this value did not exceed 16% and only in seven cases exceeded 10%. All active groups exhibiting the best impact on binding properties of ligands contain in their structure aromatic or heterocyclic rings and chemical groups which can fulfil the role of hydrogen-bond donors or acceptors. Among all considered chemical groups, only in four cases was there observed a decrease of binding affinity of ligand toward protein, each of them being an aliphatic system with hydrogen-bond donors. The use of a similar set of active groups in the R2 position meant that for 18 ligand structures there was observed an increase of affinity toward the CDK2 active site. In 14 cases it exceeded 10% and the highest reported values indicated almost a 25% increase of binding properties. The highest impact on the increase of binding affinity has substitution of active groups number 10, 9, 15, 1, 11, 13, and 12 in R2 position. The comparison of energy values characterizing all modified structures indicates that substitutions in the R2 position have a greater impact on binding affinity than modification added to R1. The next step of docking proceedings used ligand structures created with the use of active groups, which ensured at least 10% increase of binding affinity (7 substitutions R1, 14 substitutions R2). The values describing binding affinity and basic molecular descriptors for the chosen ligand molecules are presented in Table 2, and the characteristics of all structures analyzed in this work are placed in the Appendix A Table A1. During ligand selection, the used criteria encompassed not only the values of binding affinity and related inhibition constant (IC), but also molecular descriptors such as LogP and toxicity of considered molecules. The toxicity

of the analyzed compounds estimated during QSAR predictions is described by values in the range from 0 to 1. The compounds with very low toxicity adopt values from 0.0–0.2, the moderate toxic ones correspond to values 0.2–0.8, and highly toxic compounds to values 0.8–1.0, with the standard error for estimated values being 0.1. Among all considered oxindole derivatives, only 23 structures were characterized by values indicating nontoxic character. In the next stage, compounds characterized as medium toxic, with toxicity index below 0.4, were also used, which allowed an increase in the studied group to 40 compounds. The IC for ligand molecules was estimated based on the equation

$$K_I = \exp\left(\frac{\Delta G_b}{RT}\right)$$

where ΔG_b represents binding affinity, R gas constant, and T temperature. The analysis including all presented factors allows for selection of potential inhibitors characterized by small values of inhibition constant, slight toxicity, and potentially good permeability through cell membranes (LogP). The best obtained structures are characterized by ~30% increase of binding affinity toward the CDK2 binding site, which is also related to significant changes in IC, which decreased in best cases to values lower than 10 nM (IC for Indol_0_0 = 824.2 nM).

Table 1. The values of binding affinity of oxindol mono derivatives towards CDK2. Increase of binding affinity estimated relative to the value for Indol_0_0 equals -8.3 kcal/mol.

Name	Binding Affinity (kcal/mol)	Increase of Binding Affinity (%)	Name	Binding Affinity (kcal/mol)	Increase of Binding Affinity (%)
Indol_9_0	-9.6	15.7	Indol_0_10	-10.3	24.1
Indol_15_0	-9.5	14.5	Indol_0_9	-10.2	22.9
Indol_10_0	-9.4	13.3	Indol_0_15	-10.1	21.7
Indol_20_0	-9.3	12.0	Indol_0_11	-9.8	18.1
Indol_1_0	-9.3	12.0	Indol_0_1	-9.66	16.4
Indol_4_0	-9.24	11.3	Indol_0_13	-9.6	15.7
Indol_18_0	-9.22	11.1	Indol_0_12	-9.58	15.4
Indol_11_0	-9	8.4	Indol_0_4	-9.3	12.0
Indol_8_0	-8.9	7.2	Indol_0_6	-9.3	12.0
Indol_6_0	-8.9	7.2	Indol_0_19	-9.3	12.0
Indol_3_0	-8.9	7.2	Indol_0_3	-9.2	10.8
Indol_13_0	-8.9	7.2	Indol_0_5	-9.2	10.8
Indol_14_0	-8.86	6.7	Indol_0_8	-9	8.4
Indol_2_0	-8.8	6.0	Indol_0_14	-9	8.4
Indol_12_0	-8.76	5.5	Indol_0_2	-8.96	8.0
Indol_5_0	-8.74	5.3	Indol_0_18	-8.82	6.3
Indol_19_0	-8.2	-1.2	Indol_0_7	-8.8	6.0
Indol_17_0	-8.2	-1.2	Indol_0_16	-8.5	2.4
Indol_7_0	-8.02	-3.4	Indol_0_20	-8.3	0.0
Indol_16_0	-7.92	-4.6	Indol_0_17	-8.24	-0.7

The interactions involved in the stabilization of complexes of five chosen ligands exhibiting best properties are presented in Figure 3; the summary presentation of all observed interactions is attached in Table 3. For all obtained ligand molecules, characteristic interactions of oxindole derivatives created by atoms from molecule core are observed. Considering geometric classification of hydrogen-bond strength, interactions with Leu 83, Glu 81, and Lys 33 can be classified as medium-strength impacts in the case of all chosen structures, while the bonds created with Asp 146 are weak. For all considered ligands, potential stacking interactions with aromatic system of Phe 80 were also observed, and in all cases similar distances between aromatic rings and their analogical mutual orientation were noticed. The addition of active groups in the R1 and R2 positions provided additional impacts, which are hydrogen bonds with Gln 85 (all), Glu 12 (Indol_4_9; Indol_4_10), Asp 86 (Indol_20_10, Indol_20_15, Indol_4_9), Lys 89 (Indol_4_10, Indol_20_15, Indol_9_15). In all cases they can be classified as medium- or weak-strength interactions.

Table 2. The values of binding affinity and molecular parameters for the structures exhibiting the best properties.

Name	LogP	Toxicity	Binding Affinity (kcal/mol)	Increase of Binding Affinity (%)	Inhibition Constant (nM)
1. indol_20_10	3.61	0.39	-11.20	34.94	6.17
2. indol_4_10	2.04	0.07	-11.10	33.73	7.30
3. indol_4_9	3.58	0.32	-11.00	32.53	8.65
4. indol_9_15	3.64	0.19	-10.88	31.08	10.59
5. indol_20_15	2.18	0.19	-10.80	30.12	12.12
6. indol_18_12	3.85	0.28	-10.54	26.99	18.80
7. indol_18_15	1.65	0.00	-10.44	25.78	22.25
8. indol_10_4	1.58	0.08	-10.44	25.78	22.25
9. indol_18_10	2.98	0.03	-10.40	25.30	23.81
10. indol_20_4	1.46	0.11	-10.40	25.30	23.81
11. indol_4_13	1.41	0.17	-10.40	25.30	23.81
12. indol_15_12	1.95	0.30	-10.40	25.30	23.81
13. indol_4_12	2.80	0.35	-10.40	25.30	23.81
14. indol_20_1	1.26	0.39	-10.40	25.30	23.81
15. indol_10_13	3.38	0.28	-10.36	24.82	25.47

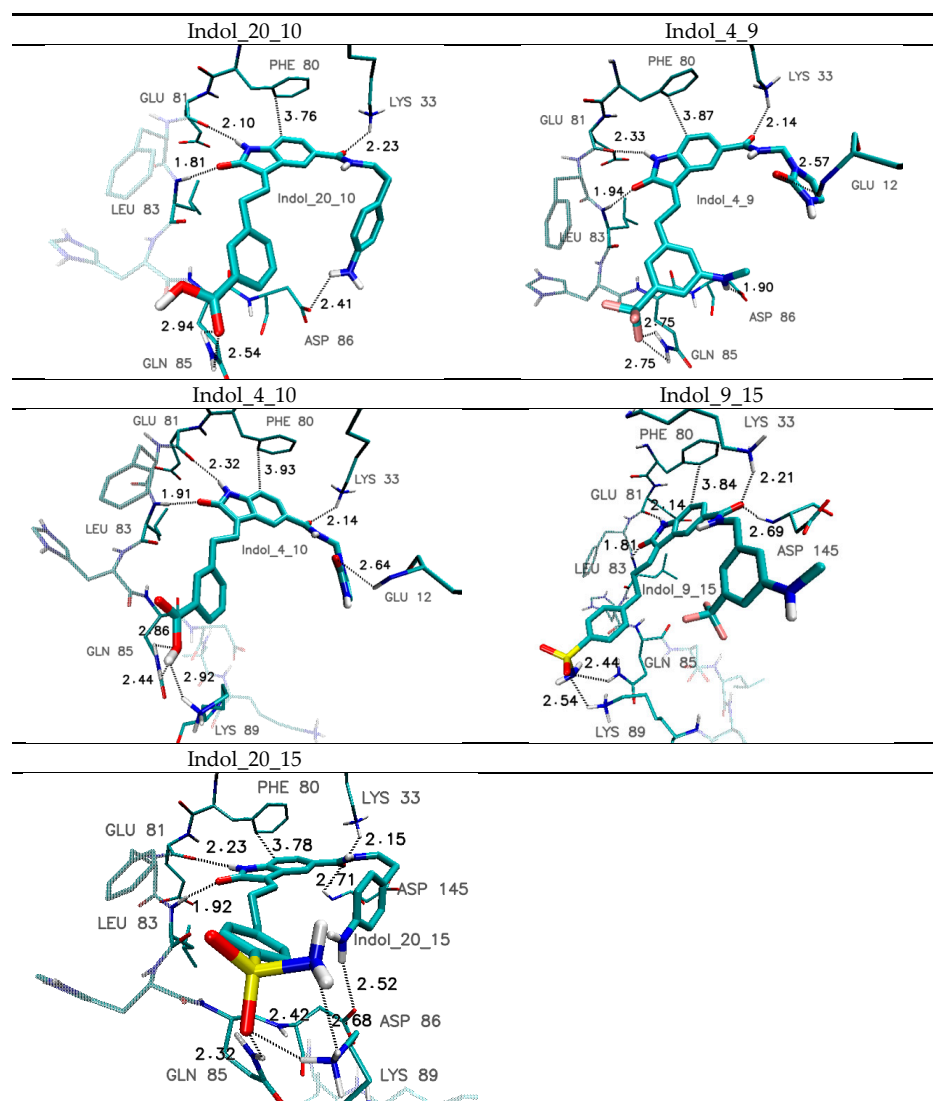
**Figure 3.** The graphic representations of interactions of chosen oxindole derivatives with CDK2 active site identified during docking stage.

Table 3. Interactions stabilizing oxindole derivatives complexes with CDK2 active site, estimated during docking simulation stage.

Amino Acid	Hydrogen-Bond Length/Distance Between Aromatic Systems * (Å)				
	Indol_4_9	Indol_4_10	Indol_9_15	Indol_20_10	Indol_20_15
Glu 12	2.57	2.64	—	—	—
Lys 33	2.14	2.14	2.21	2.23	2.15
Leu 83	1.94	1.91	1.81	1.81	1.92
Glu 81	2.33	2.32	2.14	2.10	2.23
Gln 85	2.75	2.44 2.86	2.44	2.54 2.94	2.32
Asp 86	1.90	—	—	2.41	2.52
Lys 89	—	2.92	2.54	—	2.42 2.68
Asp146	2.86	2.86	2.69	2.61	2.71
Phe 80 *	3.87	3.87	3.84	3.76	3.84

4. Molecular Dynamics of Chosen Complexes

The molecular dynamics stage of simulations covered five complexes of CDK2 protein with selected ligands characterized by best binding and molecular properties. The dynamic and structural stability of the considered systems was evaluated with the use of root mean square deviation (RMSD) values, which were estimated for protein and inhibitor molecules. The appropriate values describing each element of the analyzed complexes are presented in Figure 4 and Table 4. Each presented system reached structural equilibrium in the first 20 ns stages of the molecular dynamics simulation. The distributions and averaged values presented in the table show that CDK2 protein exhibits similar structural and dynamic properties in each considered system. The behavior of the analyzed inhibitor molecules in the protein active site is more varied. The highest structural stiffness is observed in the case of Indol_4_9 and Indol_20_10 molecules; small average values and uniform distributions indicate stable structural conformations of both inhibitors. The differences in standard deviations describing both populations are related to incidental structural fluctuations observed in the case of Indol_20_10. The rest of the considered ligand molecules are characterized by more diverse distributions. In the case of Indol_4_10, values presented on the chart indicate the potential presence of a second conformation, which appears after 30 ns of simulation time. The structures containing sulfonamide group in R2 position (Indol_9_15, Indol_20_15) exhibit higher structural flexibility than the rest of considered inhibitors, which confirms the observed fluctuations and higher standard deviations of RMSD values. The observed general trends of ligands molecule dynamic properties are also reflected in the durability of interactions involved in the stabilization of the analyzed complexes. The data presented in Table 5 describes the quantity and quality of the interactions reported for complexes during molecular dynamics simulations. Not all interactions identified during the molecular docking stage proved to be stable; however, in some cases new impacts appeared to be created with other amino acids. All realized molecular dynamics simulations revealed that interactions with Leu 83 and Glu 81 play a crucial role in the stabilization of inhibitor-CDK2 complexes. Such hydrogen bonds were observed for all conformations collected for each ligand during computations; the bond distances indicate that most can be classified as medium-strength interactions (~80% for Leu 83, ~75% for Glu 81). The third interaction created by atoms from the molecular core of the considered ligands, namely with Lys 33, is characterized by a much larger diversity, which manifests in the quantity and strength of created bonds alike. The most stable interactions are observed in the case of the Indol_4_9 molecule; however, the largest share of interactions with the highest impact energy (~40%) was recorded for Indol_9_15 and Indol_20_15 molecules. The weak interactions reported for Asp 146 disappeared

during the molecular dynamics simulation. Much more important discrepancies in relation to initial complex conformations are observed for interactions of groups placed in the side chains of considered ligands. The first considered ligand, namely Indol_4_9, creates a stable interaction with oxygen from aspartic acid ASP 86; such a hydrogen bond is observed in 98% of conformations obtained during molecular dynamics simulation. The other impacts identified during the docking procedure have changed, namely weak interactions with GLU 12 are observed only for 45% of collected conformations, while hydrogen bonds with GLN 85 have disappeared. In the case of Indol_4_10, two hydrogen bonds created by groups from side chains were observed. The first of them, created with GLU12, is observed for 46.4% of conformations, while the second impact, namely the hydrogen bond with GLU8 (69.1%), does not occur in the complex obtained during the docking phase. The appearing of this new interaction is a consequence of the change of R2 side chain conformation, which is also related to the disappearance of hydrogen bonds with LYS 98 and GLN 85. All the hydrogen bonds found for active groups from the side chains of Indol_9_15 during docking stage disappeared. The analysis of possible interactions for conformers obtained during molecular dynamics stage indicates only one hydrogen bond with GLY13; however, the quantity and distances indicate a weak stabilizing impact of this bond. The next molecule, namely Indol_20_10, interacts with the active site by hydrogen bonds created by both side chains. The hydrogen bond identified between the amino group of side chain R1 and ASP 86 is observed for 50% of conformations obtained during molecular dynamics calculations. The structural mobility of this part of ligand molecule caused the occurrence of a second competitive interaction created with the oxygen atom of ILE10 (61.3%). The active group from the second side chain also creates a bond, namely with GLU 8 (85.7%); the quantity and distance of this hydrogen bond clearly indicate a significant stabilizing impact for the complex structure. In the case of the last considered ligand, namely Indol_20_15, during the molecular dynamics stage the presence of two hydrogen bonds observed in initial complex and one new impact was identified and confirmed. Both oxygens from the sulfonamide group are involved in interactions with LYS89 (73.6%); the rotation of this group relative to the aromatic ring allowed for the appearance of a new bond observed between amide hydrogens and oxygen from HIE 84 (56.7%). The activity of the second side chain is much less significant; the hydrogen bond between amine group and ASP 86 is observed only for 48% of the conformations. The values of binding enthalpies (ΔH) obtained for complexes considered during the molecular dynamic stage strictly correspond to the dynamic properties of ligands described by RMSD values, as well as the quantity and quality of interactions involved in the stabilization of complexes. Values presented in Table 6 clearly show that the most stable complexes during molecular dynamics stage were created by two inhibitors, namely Indol_4_9 and Indol_20_10, with very similar values of enthalpy (~40 kcal/mol) and standard deviations indicating a similar inhibiting potential of these two compounds. The next group of ligands are Indol_4_10 and Indol_20_15, which are characterized by enthalpy values about 6 kcal/mol smaller than those obtained for the best inhibitors. The worst inhibiting potential among all structures analyzed during the molecular dynamics stage is shown by the Indol_9_15 molecule.

Table 4. The averaged values of RMSD (Å) for ligands and enzyme for all steps used during structural analysis. The values in italics represent standard deviations.

	Indol_4_9		Indol_4_10		Indol_9_15		Indol_20_10		Indol_20_15	
	CDK2	LIG	CDK2	LIG	CDK2	LIG	CDK2	LIG	CDK2	LIG
RMSD	2.36	1.30	2.91	1.54	2.46	1.68	2.72	0.93	2.49	1.46
SD	0.10	0.08	0.17	0.26	0.15	0.27	0.13	0.19	0.14	0.29

Table 5. Distribution of the most frequently created hydrogen bonds between ligands molecule and selected amino acids from CDK-2 active site. The hydrogen bonds in the table represent median values of intervals with a width of 0.25 Å.

Hydrogen Bond	Population %							
	Σ	1.5 Å	1.75 Å	2.0 Å	2.25 Å	2.5 Å	2.75 Å	3.0 Å
Indol_4_9								
Ligand (O2) ... (HN) LEU 83	100.0	0.0	24.1	58.9	14.8	2.1	0.1	0.0
Ligand (H3) ... (O) GLU 81	100.0	0.0	14.1	58.3	24.1	3.3	0.3	0.0
Ligand (O3) ... (H) LYS 33	98.7	0.0	24.4	44.4	16.0	8.5	2.9	2.4
Ligand (H1) ... (O) ASP 86	98.3	0.0	10.2	37.1	29.4	13.7	5.5	2.4
Ligand (H4) ... (O) GLU 12	45.4	0.0	0.1	1.4	3.6	7.9	12.7	19.7
Indol_4_10								
Ligand (O2) ... (HN) LEU 83	100.0	0.1	31.1	55.1	11.4	2.1	0.2	0.0
Ligand (H3) ... (O) GLU 81	100.0	0.0	19.5	57.2	19.1	3.3	0.9	0.0
Ligand (O3) ... (H) LYS 33	82.9	0.1	26.9	35.8	12.1	5.6	1.2	1.3
Ligand (H2) ... (O) GLU 8	69.1	15.4	43.6	8.4	1.0	0.4	0.1	0.2
Ligand (H4) ... (O) GLU 12	46.4	0.0	10.0	21.1	8.5	3.3	2.3	1.3
Indol_9_15								
Ligand (O3) ... (HN) LEU 83	100.0	0.1	24.5	55.2	17.0	2.3	0.7	0.3
Ligand (H5) ... (O) GLU 81	100.0	0.1	27.1	57.8	12.9	1.9	0.3	0.0
Ligand (O4) ... (H) LYS 33	94.3	0.2	44.3	40.5	7.3	1.5	0.3	0.3
Ligand (F) ... (H) GLY 13	31.4	0.0	0.0	0.3	1.0	3.8	9.6	16.8
Indol_20_10								
Ligand (O1) ... (HN) LEU 83	100	0.1	25.7	57.3	14.8	2.3	0.0	0.0
Ligand (H5) ... (O) GLU 81	100	0.0	27.9	56.6	13.5	1.9	0.2	0.0
Ligand (O4) ... (H) LYS 33	92.5	0.1	38.9	35.3	13.8	2.0	1.0	1.4
Ligand (NH _X) ... (O) ASP 86	50.7	0.2	18.8	22.1	5.2	1.6	1.1	1.7
Ligand (H4) ... (O) GLU 8	85.7	21.3	54.2	8.8	1.0	0.3	0.1	0.1
Ligand (NH _X) ... (O) ILE 10	61.3	0.0	10.9	25.0	11.2	4.5	4.9	4.8
Indol_20_15								
Ligand (O3) ... (HN) LEU 83	100.0	0.1	23.2	59.4	15.0	2.3	0.1	0.0
Ligand (H6) ... (O) GLU 81	100.0	0.0	24.3	61.4	13.2	0.9	0.1	0.0
Ligand (O4) ... (H) LYS 33	89.6	0.3	38.4	39.4	8.2	2.5	0.6	0.2
Ligand (H3) ... (O) ASP 86	48.0	0.0	11.4	20.0	9.0	3.3	2.6	1.7
Ligand (H1) ... (O) HIE 84	56.7	0.1	20.9	25.1	6.8	1.6	0.9	1.2
Ligand (O1/2) ... (H) LYS 89	73.6	0.1	6.7	23.5	17.6	11.8	8.5	5.4

Table 6. The values of binding enthalpy (kcal/mol) estimated for all complexes considered during molecular dynamics stage ($E_{VDWAALS}$ = van der Waals contribution from MM.; E_{EL} = electrostatic energy; E_{PB} = the electrostatic contribution to the solvation free energy calculated by PB; E_{CAVITY} = nonpolar contribution to the solvation free energy; ΔH = final estimated binding enthalpy).

	Indol_4_9		Indol_4_10		Indol_9_15		Indol_20_10		Indol_20_15	
	ΔE	SD	ΔE	SD	ΔE	SD	ΔE	SD	ΔE	SD
$E_{VDWAALS}$	-49.11	2.69	-46.55	4.11	-52.15	3.91	-49.56	5.35	-48.56	7.74
E_{EL}	-51.37	5.47	-48.50	11.03	-51.08	9.87	-48.47	8.36	-47.83	12.99
E_{PB}	64.27	6.44	65.24	8.06	77.96	8.56	63.82	5.35	70.35	11.03
E_{CAVITY}	-4.47	1.04	-4.65	1.70	-4.22	2.20	-5.11	0.19	-6.98	3.60
ΔH	-40.67	8.81	-34.47	9.02	-29.48	10.32	-39.31	8.31	-33.02	7.22

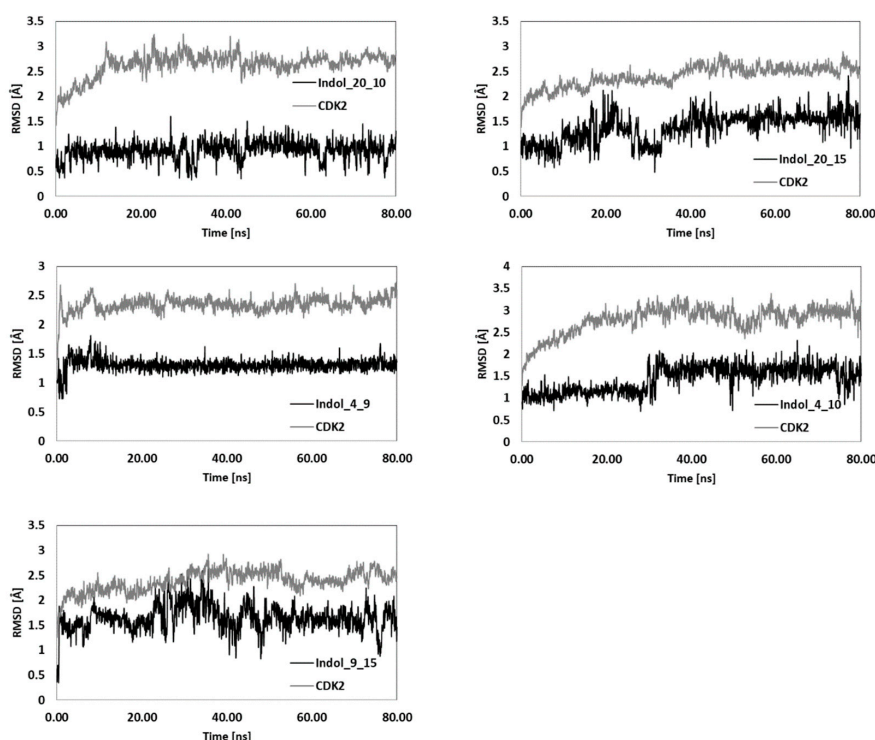


Figure 4. Distributions of RMSD (\AA) values. Black distributions refer to ligand molecules while gray distributions refer to CDK-2 protein.

5. The Immobilization of Chosen Ligands with the Use of C_{60} Fullerene Derivatives

In the last stage of research, two ligand molecules were used which exhibit the highest affinity towards active site during molecular dynamics stage, namely Indol_4_9 and Indol_20_10. The affinity of the mentioned molecules towards C_{60} fullerene and its derivatives was evaluated during docking calculations. The data presented in Tables 7 and 8 show that both considered ligands exhibit similar affinity toward native C_{60} fullerene; however, slightly higher values are denoted for the Indol_20_10 molecule. Both considered ligand molecules contain in each of their side chains one cyclic system, aromatic or heterocyclic, and such a chemical structure allows an occurrence of stacking interactions. The graphic representations of these complexes included in Figure 5 confirm that all cyclic systems of both inhibitors are involved in such a type of interaction. The planar orientation of all cyclic systems relative to fullerene surface and relatively small distances placed in the range from 3.36 to 3.77 \AA indicate an occurrence of strong stacking interactions stabilizing the considered complexes. The rest of the values presented in Tables 7 and 8 concerns functionalized derivatives of C_{60} fullerene. Each of these structures was created by a single or multiple addition of functional groups to the fullerene surface. Among all used substituents there can be found aliphatic chains with halogen, methoxy, ester, and amide groups, and aromatic systems such as unsubstituted benzene rings and more complex aromatic systems. The description of all used nanosystems is presented in Table A2. All the structural modifications observed in the considered nanocarriers contributed to an increase of binding affinities towards both ligand molecules. In the case of Indol_4_9, the observed differences are placed in a range from -0.7 to -1.8 kcal/mol while for Indol_20_10 from -0.8 to -2 kcal/mol. Much more evident discrepancies are observed in the case of binding constant for the complex creation. The comparison of the best obtained complexes relative to the reference system (C_{60} fullerene) indicates an increase in the yield of the complex formation reaching as much as 2824%. The Indol_4_9 exhibits the highest binding affinity toward FF_12 fullerene, and the increase of yield of this complex formation relative to the reference system is equal to 1986.5%. The complex obtained during the docking stage is maintained by several stacking interactions occurring between all cyclic systems of ligand and surface of fullerene;

observed distances are placed in the range from 3.26 to 3.58 Å. Also, the orientation of both cyclic systems from side chains towards aromatic substituents placed on the fullerene surface indicates the presence of additional stabilizing impacts. The next interesting complexes of this ligand are created with FF_5 and FF_11 nanomolecules; both are characterized by similar affinity values. In both complexes, all cyclic systems are involved in the creation of stacking interactions. In the case of complexes with the FF_5 molecule, a new stabilizing impact appears, namely the hydrogen bond between the hydrogen from the amine group and oxygen from the phosphoryl group with the distance of 1.96 Å, indicating the medium strength of this impact. The complexes created by Indol_20_10 are characterized by higher affinity values in relation to the previously discussed inhibitor. The most stable complexes are created with FF_12 and FF_11 nanomolecules and the value of binding affinity equals -9.2 kcal/mol, causing the yield of these complexes creation to be higher by 2824% relative to the reference system. The graphic representations presented in Figure 5 confirm that in both complexes all aromatic systems of the considered ligand create stacking interactions with fullerene surface, and in some cases also with aromatic substituents placed on the fullerene surface. The next interesting group of complexes created by Indol_20_10 are systems containing FF_3, FF_5, and FF_9 nanocarriers, all of which are characterized by similar affinity values ($-8,9$ kcal/mol). The increase of yield relative to the reference system in this case reaches a value of 1662.4%. The observed ligand conformations in all cases supports the occurrence of stacking interactions between all aromatic systems of ligand and the surface of considered nanomolecules; denoted distances are placed in the range from 3.27 to 3.8 Å.

Table 7. Values of binding affinity (kcal/mol) of Indol_4_9 molecule relative to functionalized C₆₀ fullerene derivatives (FF_X) obtained during docking stage.

Nanostructure Name	ΔG (kcal/mol)				Binding Constant (K _{max})	Difference of K _{max} Relative to C ₆₀ (%)
	MAX	MIN	AVERAGE	SD		
FF_1	-8.1	-7.6	-7.78	0.12	865722.5	657.9
FF_2	-7.9	-7.6	-7.76	0.07	617698.8	440.8
FF_3	-8.1	-7.8	-7.92	0.10	865722.5	657.9
FF_4	-7.9	-7.7	-7.76	0.07	617698.8	440.8
FF_5	-8.4	-8	-8.14	0.13	1436420.7	1157.5
FF_6	-7.9	-7.5	-7.74	0.10	617698.8	440.8
FF_7	-8	-7.8	-7.91	0.07	731270.0	540.2
FF_8	-7.9	-7.7	-7.79	0.04	617698.8	440.8
FF_9	-8.1	-7.7	-7.94	0.13	865722.5	657.9
FF_10	-7.6	-7.3	-7.47	0.08	372283.6	225.9
FF_11	-8.3	-7.7	-7.92	0.15	1213334.8	962.2
FF_12	-8.7	-8.2	-8.37	0.11	2383332.1	1986.5
FF_13	-8	-7.6	-7.80	0.13	731270.0	540.2
C ₆₀	-6.9	-6.8	-6.84	0.05	114226.6	0.0

Table 8. Values of binding affinity (kcal/mol) of Indol_20_10 molecule relative to functionalized C₆₀ fullerene derivatives (FF_X) obtained during docking stage.

Nanostructure Name	ΔG (kcal/mol)				Binding Constant (K _{max})	Difference of K _{max} Relative to C ₆₀ (%)
	MAX	MIN	AVERAGE	SD		
FF_1	-8.60	-8.10	-8.31	0.12	2013184.5	962.2
FF_2	-8.40	-7.80	-8.14	0.19	1436420.7	657.9
FF_3	-8.90	-8.30	-8.56	0.15	3340307.9	1662.4
FF_4	-8.30	-8.00	-8.15	0.09	1213334.8	540.2
FF_5	-8.90	-8.60	-8.71	0.10	3340307.9	1662.4
FF_6	-8.50	-8.10	-8.24	0.10	1700523.4	797.2
FF_7	-8.70	-8.50	-8.63	0.07	2383332.1	1157.5
FF_8	-8.70	-8.30	-8.51	0.11	2383332.1	1157.5
FF_9	-8.90	-8.30	-8.61	0.17	3340307.9	1662.4
FF_10	-8.00	-7.70	-7.89	0.12	731270.0	285.8
FF_11	-9.20	-7.80	-8.31	0.35	5542292.2	2824.3
FF_12	-9.20	-8.60	-8.86	0.19	5542292.2	2824.3
FF_13	-8.60	-8.20	-8.36	0.11	2013184.5	962.2
C ₆₀	-7.20	-7.10	-7.14	0.05	189526.5	0.0

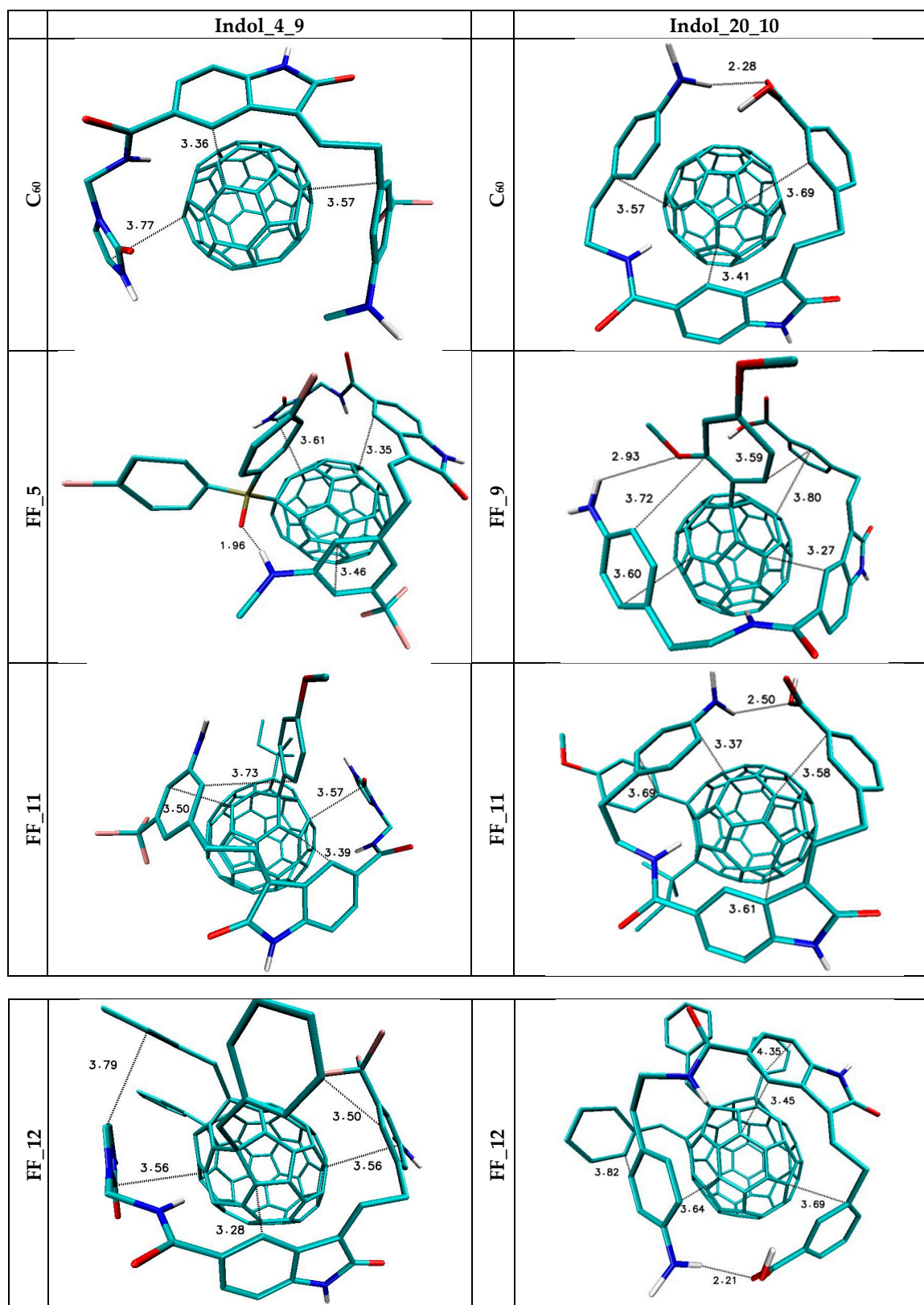


Figure 5. Graphic representation of chosen ligand complexes with functionalized derivatives of C₆₀ fullerene characterized by highest binding affinity.

6. Conclusions

The proposed procedure of oxindole derivative preparation allows indication of a group of compounds exhibiting an inhibiting potential towards the CDK2 active site. The realized calculations unambiguously show that both proposed additions to the oxindole core considerably affect the binding affinity towards the active site. The use of similar groups of substituents in both side chains allows a conclusion that modifications made in the R2 position contribute to a much greater increase of binding affinity than modifications in the R1 position. Such an observation clearly shows that this part of the active site created by amino acids LEU83, HIE84, GLN85, ASP86, LYS89, and GLU8 exhibits much more activity in the creation of interactions with ligand molecules. The greatest impact on the values of binding affinity was exerted by substituents, which were heterocyclic or aromatic systems with hydrogen-bond donors and acceptors. Among all the created structures, a significant part was compounds exhibiting not only high binding affinity toward the active site but also an acceptable level of toxicity and a satisfactory ability to penetrate cell membranes expressed by LogP values. The oxindole derivatives chosen based on these factors were evaluated during the molecular dynamics stage and almost all of them confirmed their inhibitory abilities. Two of the analyzed structures, namely Indol_4_9 and Indol_20_10, are characterized by the highest enthalpy values describing their affinities relative to the active site. The energetic aspects correlate also with structural analysis of conformers collected during the molecular dynamics stage. The stable interactions during simulation time, created not only by active groups from molecule core but also for both side chains, together with uniform distribution of RMSD values characterizing these ligands, indicate a significant stability of the considered complexes. Slightly worse but also satisfactory properties exhibit complexes formed by Indol_4_10 and Indol_20_15. Only in the case of Indol_9_15 molecular dynamics analysis was there a total disappearance of interactions created by active groups from side chains identified during the docking stage. This phenomenon is not related to the appearance of new competitive interactions. Such structural observations also confirm a significant decrease of binding enthalpy. The realized calculations show that the best oxindole derivatives exhibit significant affinity towards C₆₀ fullerene and functionalized derivatives of this nanomolecule. The three cyclic systems in each of the molecules consist of aromatic or heterocyclic groups which can participate in π - π stacking interactions with fullerene surface. The obtained data shows that the most significant increase of binding affinity is related to the presence of additional aromatic substituents on the fullerene surface as confirmed by values characterizing ligand complexes with FF_12 and FF_11 fullerene. The obtained data shows that one of the most important factors stabilizing such complexes is stacking and hydrophobic interactions; the presence of hydrogen-bond donors or acceptors does not play such an important role in the stabilization of such complexes. The presented data clearly shows that the created complexes of oxindole derivatives and considered nanocarriers exhibit significant potential in the creation of immobilized drugs, and can be used in the development of targeted therapies.

Funding: This research received no external funding.

Acknowledgments: This research was supported by PL-Grid Infrastructure (<http://www.plgrid.pl/en>).

Conflicts of Interest: The author declares that there are no conflicts of interest.

Appendix A

Table A1. The characteristics of affinities and molecular descriptors of analyzed oxindole derivatives. (ΔG —ligand binding affinity; IC—Inhibition constant; Tox—index of toxicity; LogP—octanol/water coefficient; MW—molecular weight; n HbA—number of hydrogen-bond acceptors; n HbD—number of hydrogen-bond donors.).

Name	SMILES	ΔG (kcal/mol)	IC (nM)	Tox	LogP	MW (g/mol)	n HbA	n HbD
<i>indol_1_10</i>	<chem>c12c(cc(cc1)C(=O)NCc1nonc1N)/C(=C/Cc1cc(ccc1)C(=O)O)/C(=O)N2</chem>	-11	8.65	0.8	2.056	419.4	10	5
<i>indol_1_11</i>	<chem>c12c(cc(cc1)C(=O)NCc1nonc1N)/C(=C/Cc1ccnc(n1)N)/C(=O)N2</chem>	-10.66	15.35	0.93	0.074	392.38	11	6
<i>indol_1_12</i>	<chem>c12c(cc(cc1)C(=O)NCc1nonc1N)/C(=C/CNc1ccc(cc1)Br)/C(=O)N2</chem>	-10.48	20.80	0.9	2.85	469.3	9	5
<i>indol_1_13</i>	<chem>c12c(cc(cc1)C(=O)NCc1nonc1N)/C(=C/CC1CCNCC1)/C(=O)N2</chem>	-10.3	28.18	0.86	1.692	382.42	9	5
<i>indol_1_15</i>	<chem>c12c(cc(cc1)C(=O)NCc1nonc1N)/C(=C/CCc1ccc(cc1)S(=O)(=O)N)/C(=O)N2</chem>	-10.04	43.71	0.84	0.416	468.5	11	6
<i>indol_1_19</i>	<chem>c12c(cc(cc1)C(=O)NCc1nonc1N)/C(=C/CNC(=O)c1ccccc1)/C(=O)N2</chem>	-9.56	98.27	0.75	1.136	418.41	10	5
<i>indol_1_3</i>	<chem>c12c(cc(cc1)C(=O)NCc1nonc1N)/C(=C/Cc1nc[nH]c1)/C(=O)N2</chem>	-10.00	46.76	0.94	0.465	365.35	10	5
<i>indol_1_4</i>	<chem>c12c(cc(cc1)C(=O)NCc1nonc1N)/C(=C/Cn1c(=O)[nH]cc1)/C(=O)N2</chem>	-10.1	39.50	0.97	-0.015	381.35	11	5
<i>indol_1_5</i>	<chem>c12c(cc(cc1)C(=O)NCc1nonc1N)/C(=C/CC1=CC(=NC1=O)NC)/C(=O)N2</chem>	-9.62	88.81	0.92	-1.075	407.39	11	5
<i>indol_1_6</i>	<chem>c12c(cc(cc1)C(=O)NCc1nonc1N)/C(=C/Cc1enc[nH]1)/C(=O)N2</chem>	-10.1	39.50	0.94	0.227	365.35	10	5
<i>indol_1_9</i>	<chem>c12c(cc(cc1)C(=O)NCc1nonc1N)/C(=C/Cc1cc(cc(c1)NC)C(F)F)/C(=O)N2</chem>	-11.08	7.56	0.89	3.527	472.43	9	5
<i>indol_4_1</i>	<chem>c12c(cc(cc1)C(=O)NCn1c(=O)[nH]cc1)/C(=C/CCc1nonc1N)/C(=O)N2</chem>	-10.2	33.37	0.97	0.314	395.38	11	5
<i>indol_4_10</i>	<chem>c12c(cc(cc1)C(=O)NCn1c(=O)[nH]cc1)/C(=C/Cc1cc(ccc1)C(=O)O)/C(=O)N2</chem>	-11.1	7.30	0.07	2.043	418.41	9	4
<i>indol_4_11</i>	<chem>c12c(cc(cc1)C(=O)NCn1c(=O)[nH]cc1)/C(=C/Cc1ccnc(n1)N)/C(=O)N2</chem>	-10.7	14.35	0.88	-0.012	391.39	10	5
<i>indol_4_12</i>	<chem>c12c(cc(cc1)C(=O)NCn1c(=O)[nH]cc1)/C(=C/CNc1ccc(cc1)Br)/C(=O)N2</chem>	-10.4	23.81	0.35	2.801	468.31	8	4
<i>indol_4_13</i>	<chem>c12c(cc(cc1)C(=O)NCn1c(=O)[nH]cc1)/C(=C/CC1CCNCC1)/C(=O)N2</chem>	-10.4	23.81	0.17	1.408	381.44	8	4
<i>indol_4_15</i>	<chem>c12c(cc(cc1)C(=O)NCn1c(=O)[nH]cc1)/C(=C/CCc1ccc(cc1)S(=O)(=O)N)/C(=O)N2</chem>	-10.72	13.87	0.01	0.445	467.51	10	5
<i>indol_4_19</i>	<chem>c12c(cc(cc1)C(=O)NCn1c(=O)[nH]cc1)/C(=C/CNC(=O)c1ccccc1)/C(=O)N2</chem>	-9.28	157.64	0	0.855	417.43	9	4
<i>indol_4_3</i>	<chem>c12c(cc(cc1)C(=O)NCn1c(=O)[nH]cc1)/C(=C/Cc1nc[nH]c1)/C(=O)N2</chem>	-10	46.76	0.76	0.405	364.37	9	4
<i>indol_4_5</i>	<chem>c12c(cc(cc1)C(=O)NCn1c(=O)[nH]cc1)/C(=C/CC1=CC(=NC1=O)NC)/C(=O)N2</chem>	-9.66	83.01	0.43	-1.317	406.4	10	4
<i>indol_4_6</i>	<chem>c12c(cc(cc1)C(=O)NCn1c(=O)[nH]cc1)/C(=C/Cc1enc[nH]1)/C(=O)N2</chem>	-10.02	45.21	0.76	0.031	364.37	9	4
<i>indol_4_9</i>	<chem>c12c(cc(cc1)C(=O)NCn1c(=O)[nH]cc1)/C(=C/Cc1cc(cc(c1)NC)C(F)F)/C(=O)N2</chem>	-11	8.65	0.32	3.579	471.44	8	4
<i>indol_9_1</i>	<chem>c12c(cc(cc1)C(=O)NCc1cc(cc(c1)NC)C(F)F)/C(=C/CCc1nonc1N)/C(=O)N2</chem>	-9.6	91.86	0.88	3.562	486.45	9	5
<i>indol_9_10</i>	<chem>c12c(cc(cc1)C(=O)NCc1cc(cc(c1)NC)C(F)F)/C(=C/Cc1cc(ccc1)C(=O)O)/C(=O)N2</chem>	-10.54	18.80	0.39	5.116	509.48	7	4
<i>indol_9_11</i>	<chem>c12c(cc(cc1)C(=O)NCc1cc(cc(c1)NC)C(F)F)/C(=C/Cc1ccnc(n1)N)/C(=O)N2</chem>	-10.24	31.19	0.69	3.281	482.47	8	5
<i>indol_9_12</i>	<chem>c12c(cc(cc1)C(=O)NCc1cc(cc(c1)NC)C(F)F)/C(=C/CNc1ccc(cc1)Br)/C(=O)N2</chem>	-9.72	75.01	0.59	5.9	559.39	6	4
<i>indol_9_13</i>	<chem>c12c(cc(cc1)C(=O)NCc1cc(cc(c1)NC)C(F)F)/C(=C/CC1CCNCC1)/C(=O)N2</chem>	-10.22	32.26	0.45	4.809	472.51	6	4

Table A1. Cont.

Name	SMILES	ΔG (kcal/mol)	IC (nM)	Tox	LogP	MW (g/mol)	n HbA	n HbD
<i>indol_9_15</i>	<chem>c12c(cc(cc1)C(=O)NCc1cc(cc(c1)NC)C(F)(F)F)/C(=C/CCc1ccc(cc1)S(=O)(=O)N)/C(=O)N2</chem>	-10.58	17.57	0.19	3.644	558.58	8	5
<i>indol_9_19</i>	<chem>c12c(cc(cc1)C(=O)NCc1cc(cc(c1)NC)C(F)(F)F)/C(=C/CNC(=O)c1ccccc1)/C(=O)N2</chem>	-9.72	75.01	0.11	4.076	508.5	7	4
<i>indol_9_3</i>	<chem>c12c(cc(cc1)C(=O)NCc1cc(cc(c1)NC)C(F)(F)F)/C(=C/Cc1nc[nH]c1)/C(=O)N2</chem>	-9.9	55.36	0.66	3.694	455.44	7	4
<i>indol_9_4</i>	<chem>c12c(cc(cc1)C(=O)NCc1cc(cc(c1)NC)C(F)(F)F)/C(=C/Cn1c(=O)[nH]cc1)/C(=O)N2</chem>	-10.08	40.86	0.24	2.923	471.44	8	4
<i>indol_9_5</i>	<chem>c12c(cc(cc1)C(=O)NCc1cc(cc(c1)NC)C(F)(F)F)/C(=C/CC1=CC(=NC1=O)NC)/C(=O)N2</chem>	-9.86	59.23	0.36	2.07	497.48	8	4
<i>indol_9_6</i>	<chem>c12c(cc(cc1)C(=O)NCc1cc(cc(c1)NC)C(F)(F)F)/C(=C/Cc1cnc[nH]1)/C(=O)N2</chem>	-9.92	53.52	0.67	3.455	455.44	7	4
<i>indol_10_1</i>	<chem>c12c(cc(cc1)C(=O)NCc1cc(ccc1)C(=O)O)/C(=C/CCc1nonc1N)/C(=O)N2</chem>	-9.54	101.65	0.79	2.235	433.42	10	5
<i>indol_10_11</i>	<chem>c12c(cc(cc1)C(=O)NCc1cc(ccc1)C(=O)O)/C(=C/Cc1cenc(n1)N)/C(=O)N2</chem>	-10.7	14.35	0.4	1.66	429.44	9	5
<i>indol_10_12</i>	<chem>c12c(cc(cc1)C(=O)NCc1cc(ccc1)C(=O)O)/C(=C/CNc1ccc(cc1)Br)/C(=O)N2</chem>	-10.16	35.70	0.51	4.497	506.36	7	4
<i>indol_10_13</i>	<chem>c12c(cc(cc1)C(=O)NCc1cc(ccc1)C(=O)O)/C(=C/CC1CCNCC1)/C(=O)N2</chem>	-10.36	25.47	0.28	3.377	419.48	7	4
<i>indol_10_15</i>	<chem>c12c(cc(cc1)C(=O)NCc1cc(ccc1)C(=O)O)/C(=C/CCc1ccc(cc1)S(=O)(=O)N)/C(=O)N2</chem>	-10.58	17.57	0.45	2.318	505.55	9	5
<i>indol_10_19</i>	<chem>c12c(cc(cc1)C(=O)NCc1cc(ccc1)C(=O)O)/C(=C/CNC(=O)c1ccccc1)/C(=O)N2</chem>	-9.3	152.41	0.03	2.936	455.47	8	4
<i>indol_10_3</i>	<chem>c12c(cc(cc1)C(=O)NCc1cc(ccc1)C(=O)O)/C(=C/Cc1nc[nH]c1)/C(=O)N2</chem>	-10.18	34.51	0.46	2.176	402.41	8	4
<i>indol_10_4</i>	<chem>c12c(cc(cc1)C(=O)NCc1cc(ccc1)C(=O)O)/C(=C/Cn1c(=O)[nH]cc1)/C(=O)N2</chem>	-10.44	22.25	0.08	1.582	418.41	9	4
<i>indol_10_5</i>	<chem>c12c(cc(cc1)C(=O)NCc1cc(ccc1)C(=O)O)/C(=C/CC1=CC(=NC1=O)NC)/C(=O)N2</chem>	-9.98	48.37	0.15	0.749	444.45	9	4
<i>indol_10_6</i>	<chem>c12c(cc(cc1)C(=O)NCc1cc(ccc1)C(=O)O)/C(=C/Cc1cnc[nH]1)/C(=O)N2</chem>	-10.16	35.70	0.45	1.903	402.41	8	4
<i>indol_10_9</i>	<chem>c12c(cc(cc1)C(=O)NCc1cc(ccc1)C(=O)O)/C(=C/Cc1cc(cc(c1)NC)C(F)(F)F)/C(=O)N2</chem>	-10.88	10.59	0.46	5.274	509.48	7	4
<i>indol_15_1</i>	<chem>c12c(cc(cc1)C(=O)NCc1ccc(cc1)S(=O)(=O)N)/C(=C/CCc1nonc1N)/C(=O)N2</chem>	-10.08	40.86	0.87	-1.335	468.5	11	6
<i>indol_15_10</i>	<chem>c12c(cc(cc1)C(=O)NCc1ccc(cc1)S(=O)(=O)N)/C(=C/Cc1cc(ccc1)C(=O)O)/C(=O)N2</chem>	-10.78	12.54	0.49	0.998	491.52	9	5
<i>indol_15_11</i>	<chem>c12c(cc(cc1)C(=O)NCc1ccc(cc1)S(=O)(=O)N)/C(=C/Cc1cenc(n1)N)/C(=O)N2</chem>	-10.48	20.80	0.24	-0.85	464.51	10	6
<i>indol_15_12</i>	<chem>c12c(cc(cc1)C(=O)NCc1ccc(cc1)S(=O)(=O)N)/C(=C/CNc1ccc(cc1)Br)/C(=O)N2</chem>	-10.4	23.81	0.3	1.952	541.43	8	5
<i>indol_15_13</i>	<chem>c12c(cc(cc1)C(=O)NCc1ccc(cc1)S(=O)(=O)N)/C(=C/CC1CCNCC1)/C(=O)N2</chem>	-10.08	40.86	0.14	0.662	454.55	8	5
<i>indol_15_19</i>	<chem>c12c(cc(cc1)C(=O)NCc1ccc(cc1)S(=O)(=O)N)/C(=C/CNC(=O)c1ccccc1)/C(=O)N2</chem>	-10.28	29.15	0.01	0.095	490.54	9	5
<i>indol_15_3</i>	<chem>c12c(cc(cc1)C(=O)NCc1ccc(cc1)S(=O)(=O)N)/C(=C/Cc1nc[nH]c1)/C(=O)N2</chem>	-10	46.76	0.29	-0.86	437.48	9	5
<i>indol_15_4</i>	<chem>c12c(cc(cc1)C(=O)NCc1ccc(cc1)S(=O)(=O)N)/C(=C/Cn1c(=O)[nH]cc1)/C(=O)N2</chem>	-10.2	33.37	0.01	-1.221	453.48	10	5
<i>indol_15_5</i>	<chem>c12c(cc(cc1)C(=O)NCc1ccc(cc1)S(=O)(=O)N)/C(=C/CC1=CC(=NC1=O)NC)/C(=O)N2</chem>	-9.1	213.61	0.02	-2.226	479.52	10	5
<i>indol_15_6</i>	<chem>c12c(cc(cc1)C(=O)NCc1ccc(cc1)S(=O)(=O)N)/C(=C/Cc1cnc[nH]1)/C(=O)N2</chem>	-10.02	45.21	0.27	-0.753	437.48	9	5
<i>indol_15_9</i>	<chem>c12c(cc(cc1)C(=O)NCc1ccc(cc1)S(=O)(=O)N)/C(=C/Cc1cc(cc(c1)NC)C(F)(F)F)/C(=O)N2</chem>	-9.36	137.73	0.25	2.576	544.55	8	5
<i>indol_18_1</i>	<chem>c12c(cc(cc1)C(=O)N(C(=O)Nc1ccccc1)C)/C(=C/CCc1nonc1N)/C(=O)N2</chem>	-9.88	57.26	0.94	0.754	432.44	10	4
<i>indol_18_10</i>	<chem>c12c(cc(cc1)C(=O)N(C(=O)Nc1ccccc1)C)/C(=C/Cc1cc(ccc1)C(=O)O)/C(=O)N2</chem>	-10.88	10.59	0.03	2.979	455.47	8	3
<i>indol_18_11</i>	<chem>c12c(cc(cc1)C(=O)N(C(=O)Nc1ccccc1)C)/C(=C/Cc1cenc(n1)N)/C(=O)N2</chem>	-10.52	19.44	0.7	1.089	428.45	9	4
<i>indol_18_12</i>	<chem>c12c(cc(cc1)C(=O)N(C(=O)Nc1ccccc1)C)/C(=C/CNc1ccc(cc1)Br)/C(=O)N2</chem>	-10.54	18.80	0.28	3.852	505.37	7	3
<i>indol_18_13</i>	<chem>c12c(cc(cc1)C(=O)N(C(=O)Nc1ccccc1)C)/C(=C/CC1CCNCC1)/C(=O)N2</chem>	-9.62	88.81	0.11	2.613	418.5	7	3

Table A1. Cont.

Name	SMILES	ΔG (kcal/mol)	IC (nM)	Tox	LogP	MW (g/mol)	n HbA	n HbD
<i>indol_18_15</i>	<chem>c12c(cc(cc1)C(=O)N(C(=O)Nc1ccccc1)C)/C(=C/CCc1ccc(cc1)S(=O)(=O)N)/C(=O)N2</chem>	-10.44	22.25	0	1.649	504.57	9	4
<i>indol_18_19</i>	<chem>c12c(cc(cc1)C(=O)N(C(=O)Nc1ccccc1)C)/C(=C/CNC(=O)c1ccccc1)/C(=O)N2</chem>	-9.16	193.03	0	1.9	454.49	8	3
<i>indol_18_3</i>	<chem>c12c(cc(cc1)C(=O)N(C(=O)Nc1ccccc1)C)/C(=C/Cc1nc[nH]c1)/C(=O)N2</chem>	-9.86	59.23	0.57	1.49	401.43	8	3
<i>indol_18_4</i>	<chem>c12c(cc(cc1)C(=O)N(C(=O)Nc1ccccc1)C)/C(=C/Cn1c(=O)[nH]cc1)/C(=O)N2</chem>	-10.06	42.26	0.06	0.688	417.43	9	3
<i>indol_18_5</i>	<chem>c12c(cc(cc1)C(=O)N(C(=O)Nc1ccccc1)C)/C(=C/CC1=CC(=NC1=O)NC)/C(=O)N2</chem>	-9.76	70.12	0.12	0.137	443.46	9	3
<i>indol_18_6</i>	<chem>c12c(cc(cc1)C(=O)N(C(=O)Nc1ccccc1)C)/C(=C/Cc1cnc[nH]1)/C(=O)N2</chem>	-10.07	41.20	0.56	1.264	401.43	8	3
<i>indol_18_9</i>	<chem>c12c(cc(cc1)C(=O)N(C(=O)Nc1ccccc1)C)/C(=C/Cc1cc(cc1)NC)C(F)(F)F)/C(=O)N2</chem>	-10.34	26.34	0.21	4.55	508.5	7	3
<i>indol_20_1</i>	<chem>c12c(cc(cc1)C(=O)NCCc1ccc(cc1)N)/C(=C/Cc1cc(cc1)C(=O)O)/C(=O)N2</chem>	-10.4	23.81	0.39	1.261	441.49	7	5
<i>indol_20_10</i>	<chem>c12c(cc(cc1)C(=O)NCCc1ccc(cc1)N)/C(=C/Cc1cc(cc1)C(=O)O)/C(=O)N2</chem>	-11.2	6.17	0.39	3.606	441.49	7	5
<i>indol_20_11</i>	<chem>c12c(cc(cc1)C(=O)NCCc1ccc(cc1)N)/C(=C/Cc1cnc(n1)N)/C(=O)N2</chem>	-10.7	14.35	0.46	1.814	414.47	8	6
<i>indol_20_12</i>	<chem>c12c(cc(cc1)C(=O)NCCc1ccc(cc1)N)/C(=C/CNc1ccc(cc1)Br)/C(=O)N2</chem>	-10.4	23.81	0.54	4.528	491.39	6	5
<i>indol_20_13</i>	<chem>c12c(cc(cc1)C(=O)NCCc1ccc(cc1)N)/C(=C/CC1CCNCC1)/C(=O)N2</chem>	-10.6	16.99	0.4	3.151	404.51	6	5
<i>indol_20_15</i>	<chem>c12c(cc(cc1)C(=O)NCCc1ccc(cc1)N)/C(=C/CCc1ccc(cc1)S(=O)(=O)N)/C(=O)N2</chem>	-10.8	12.12	0.19	2.184	490.58	8	6
<i>indol_20_19</i>	<chem>c12c(cc(cc1)C(=O)NCCc1ccc(cc1)N)/C(=C/CNC(=O)c1ccccc1)/C(=O)N2</chem>	-9.9	55.36	0.1	2.488	440.5	7	5
<i>indol_20_3</i>	<chem>c12c(cc(cc1)C(=O)NCCc1ccc(cc1)N)/C(=C/Cc1nc[nH]c1)/C(=O)N2</chem>	-10.3	28.18	0.49	2.065	387.44	7	5
<i>indol_20_4</i>	<chem>c12c(cc(cc1)C(=O)NCCc1ccc(cc1)N)/C(=C/Cn1c(=O)[nH]cc1)/C(=O)N2</chem>	-10.4	23.81	0.11	1.461	403.44	8	5
<i>indol_20_5</i>	<chem>c12c(cc(cc1)C(=O)NCCc1ccc(cc1)N)/C(=C/CC1=CC(=NC1=O)NC)/C(=O)N2</chem>	-9.88	57.26	0.16	0.231	429.48	8	5
<i>indol_20_6</i>	<chem>c12c(cc(cc1)C(=O)NCCc1ccc(cc1)N)/C(=C/Cc1cnc[nH]1)/C(=O)N2</chem>	-10.28	29.15	0.49	1.849	387.44	7	5
<i>indol_20_9</i>	<chem>c12c(cc(cc1)C(=O)NCCc1ccc(cc1)N)/C(=C/Cc1cc(cc1)NC)C(F)(F)F)/C(=O)N2</chem>	-10.88	10.59	0.5	5.415	494.52	6	5

Table A2. Description of functionalized C₆₀ fullerene derivatives (FF_X) used during docking stage.

FF_1	CID_11332103
	C ₆₇ H ₁₄ F ₃ O ₄ P
	1-(diethoxyphosphorylmethyl)-7-(2,2,2-trifluoroethoxy)(C ₆₀ -I _h)[5,6]fullerene
FF_2	CID_11468612
	C ₆₅ H ₁₃ O ₃ P
	9-(diethoxyphosphorylmethyl)-1H-(C ₆₀ -I _h)[5,6]fullerene
FF_3	CID_16146387
	C ₆₇ H ₁₆ O ₂ Si
	methyl 9-(2-trimethylsilylethyl)(C ₆₀ -I _h)[5,6]fullerene-1-carboxylate
FF_4	CID_16150529
	C ₇₀ H ₂₀ N ₂ O ₂
	1-N,1-N,9-N,9-N-tetraethyl(C ₆₀ -I _h)[5,6]fullerene-1,9-dicarboxamide
FF_5	CID_16156307
	C ₇₂ H ₉ F ₂ OP
	9-bis(4-fluorophenyl)phosphoryl-1H-(C ₆₀ -I _h)[5,6]fullerene
FF_6	CID_53469305
	C ₆₄ H ₁₁ O ₃ P
	9-diethoxyphosphoryl-1H-(C ₆₀ -I _h)[5,6]fullerene
FF_7	CID_71618962
	C ₆₈ H ₁₀ O ₂
	9-(3,5-dimethoxyphenyl)-1H-(C ₆₀ -I _h)[5,6]fullerene
FF_8	CID_71619055
	C ₆₈ H ₁₀ O ₂
	9-(2,6-dimethoxyphenyl)-1H-(C ₆₀ -I _h)[5,6]fullerene
FF_9	CID_71619159
	C ₆₈ H ₁₀ O ₂
	9-(2,4-dimethoxyphenyl)-1H-(C ₆₀ -I _h)[5,6]fullerene
FF_10	CID_101218232
	C ₆₃ H ₄ ClF ₃ O
	1-(chloromethyl)-7-(2,2,2-trifluoroethoxy)(C ₆₀ -I _h)[5,6]fullerene
FF_11	CID_101218236
	C ₆₉ H ₉ Cl ₃ O
	1-(4-methoxyphenyl)-7-(1,1,2-trichloroethyl)(C ₆₀ -I _h)[5,6]fullerene
FF_12	CID_101266715
	C ₈₀ H ₂₂
	12,15-dibenzyl-9-phenyl-6,18-dihydro-1H-(C ₆₀ -I _h)[5,6]fullerene
FF_13	CID_101382121
	C ₆₂ F ₆
	1,9-bis(trifluoromethyl)(C ₆₀ -I _h)[5,6]fullerene

References

1. Besson, A.; Dowdy, S.F. Roberts JM CDK Inhibitors: Cell Cycle Regulators and Beyond. *Dev. Cell* **2008**, *14*, 159–169. [[CrossRef](#)] [[PubMed](#)]
2. Malumbres, M.; Barbacid M Cell cycle, CDKs and cancer: A changing paradigm. *Nat. Rev. Cancer* **2009**, *9*, 153–166. [[CrossRef](#)] [[PubMed](#)]
3. Morgan, D.O. CYCLIN-DEPENDENT KINASES: Engines, Clocks, and Microprocessors. *Annu. Rev. Cell Dev. Biol.* **1997**, *13*, 261–291. [[CrossRef](#)] [[PubMed](#)]
4. Malumbres, M.; Barbacid, M. To cycle or not to cycle: A critical decision in cancer. *Nat. Rev. Cancer* **2001**, *1*, 222–231. [[CrossRef](#)] [[PubMed](#)]
5. Child, E.S.; Hendrychová, T.; McCague, K.; Futreal, A.; Otyepka, M.; Mann, D.J. A cancer-derived mutation in the PSTAIRE helix of cyclin-dependent kinase 2 alters the stability of cyclin binding. *Biochim. Biophys. Acta. Mol. Cell Res.* **2010**, *1803*, 858–864. [[CrossRef](#)]
6. Echalié, A.; Hole, A.J.; Lolli, G.; Endicott, J.A.; Noble, M.E. An Inhibitor's-Eye View of the ATP-Binding Site of CDKs in Different Regulatory States. *ACS Chem. Biol.* **2014**, *9*, 1251–1256. [[CrossRef](#)] [[PubMed](#)]
7. Canavese, M.; Santo, L.; Raje, N. Cyclin dependent kinases in cancer. *Cancer Biol. Ther.* **2012**, *13*, 451–457. [[CrossRef](#)]
8. LEE, M.Y.; Liu, Y.W.; Chen, M.H.; Wu, J.Y.; Ho, H.Y.; Wang, Q.F.; Chuang, J.J. Indirubin-3'-monoxime promotes autophagic and apoptotic death in JM1 human acute lymphoblastic leukemia cells and K562 human chronic myelogenous leukemia cells. *Oncol. Rep.* **2013**, *29*, 2072–2078. [[CrossRef](#)]
9. Hoessel, R.; Leclerc, S.; Endicott, J.A.; Nobel, M.E.; Lawrie, A.; Tunnah, P.; Niederberger, E. Indirubin the active constituent of a Chinese antileukaemia medicine, inhibits cyclin-dependent kinases. *Nat. Cell Biol.* **1999**, *1*, 60–67. [[CrossRef](#)]
10. Shin, E.K.; Kim, J.K. Indirubin derivative E804 inhibits angiogenesis. *BMC Cancer* **2012**, *12*, 164. [[CrossRef](#)]
11. Marko, D.; Schätzle, S.; Friedel, A.; Genzlinger, A.; Zankl, H.; Meijer, L.; Eisenbrand, G. Inhibition of cyclin-dependent kinase 1 (CDK1) by indirubin derivatives in human tumour cells. *Br. J. Cancer* **2012**, *84*, 283–289. [[CrossRef](#)]
12. Martin, L.; Magnaudeix, A.; Wilson, C.M.; Yardin, C.; Terro, F. The new indirubin derivative inhibitors of glycogen synthase kinase-3, 6-BIDECO and 6-BIMYEO, prevent tau phosphorylation and apoptosis induced by the inhibition of protein phosphatase-2A by okadaic acid in cultured neurons. *J. Neurosci. Res.* **2011**, *89*, 1802–1811. [[CrossRef](#)]
13. Leclerc, S.; Garnier, M.; Hoessel, R.; Marko, D.; Bibb, J.A.; Snyder, G.L.; Eisenbrand, G. Indirubins Inhibit Glycogen Synthase Kinase-3beta and CDK5/P25, Two Protein Kinases Involved in Abnormal Tau Phosphorylation in Alzheimer's Disease. A PROPERTY COMMON TO MOST CYCLIN-DEPENDENT KINASE INHIBITORS? *J. Biol. Chem.* **2001**, *276*, 251–260. [[CrossRef](#)]
14. Beauchard, A.; Ferandin, Y.; Frère, S.; Lozach, O.; Blairvacq, M.; Meijer, L.; Besson, T. Synthesis of novel 5-substituted indirubins as protein kinases inhibitors. *Bioorg. Med. Chem.* **2006**, *14*, 6434–6443. [[CrossRef](#)]
15. Dermatakis, A.; Luk, K.C.; DePinto, W. Synthesis of potent oxindole CDK2 inhibitors. *Bioorg. Med. Chem.* **2003**, *11*, 1873–1881. [[CrossRef](#)]
16. Luk, K.C.; Simcox, M.E.; Schutt, A.; Rowan, K.; Thompson, T.; Chen, Y.; Dermatakis, A. A new series of potent oxindole inhibitors of CDK2. *Bioorg. Med. Chem. Lett.* **2004**, *14*, 913–917. [[CrossRef](#)]
17. Czeleń, P. Molecular dynamics study on inhibition mechanism of CDK-2 and GSK-3β by CHEMBL272026 molecule. *Struct. Chem.* **2016**, *27*, 1807–1818. [[CrossRef](#)]
18. Czeleń, P. Inhibition mechanism of CDK-2 and GSK-3β by a sulfamoylphenyl derivative of indoline—A molecular dynamics study. *J. Mol. Model.* **2017**, *23*, 230. [[CrossRef](#)]
19. Czeleń, P.; Szeffler, B. The Immobilization of Oxindole Derivatives with Use of Cube Rhombellane Homeomorphs. *Symmetry* **2019**, *11*, 900.
20. Szeffler, B.; Czeleń, P. Docking of Cisplatin on Fullerene Derivatives and Some Cube Rhombellane Functionalized Homeomorphs. *Symmetry* **2019**, *11*, 874. [[CrossRef](#)]
21. Szeffler, B.; Czeleń, P.; Diudea, M.V. Docking of indolizine derivatives on cube rhombellane functionalized homeomorphs. *Stud. Univ. Babeş-Bolyai Chem.* **2018**, *63*, 7–18. [[CrossRef](#)]

22. Morgen, M.; Bloom, C.; Beyerinck, R.; Bello, A.; Song, W.; Wilkinson, K.; Shamblin, S. Polymeric Nanoparticles for Increased Oral Bioavailability and Rapid Absorption Using Celecoxib as a Model of a Low-Solubility, High-Permeability Drug. *Pharm. Res.* **2012**, *29*, 427–440. [CrossRef]
23. De Jong, W.H.; Borm, P.J.A. Drug delivery and nanoparticles: applications and hazards. *Int. J. Nanomed.* **2008**, *3*, 133–149. [CrossRef]
24. Gao, Z.; Zhang, L.; Sun, Y. Nanotechnology applied to overcome tumor drug resistance. *J. Control. Release* **2012**, *162*, 45–55. [CrossRef]
25. Turov, V.V.; Chahun, V.F.; Barvinchenko, V.N.; Krupskaya, T.V.; Prylutsky, Y.I.; Scharff, P.; Ritter, U. Low-temperature ¹H-NMR spectroscopic study of doxorubicin influence on the hydrated properties of nanosilica modified by DNA. *J. Mater. Sci. Mater. Med.* **2011**, *22*, 525–532. [CrossRef]
26. Szeffler, B. Nanotechnology, from quantum mechanical calculations up to drug delivery. *Int. J. Nanomed.* **2018**, *13*, 6143–6176. [CrossRef]
27. Cataldo, F.; Da Ros, T. *Medicinal Chemistry and Pharmacological Potential of Fullerenes and Carbon Nanotubes*; Springer: Amsterdam, The Netherlands, 2008.
28. Panchuk, R.R.; Prylutska, S.V.; Chumak, V.V.; Skorokhyd, N.R.; Lehka, L.V.; Evstigneev, M.P.; Ritter, U. Application of C60 Fullerene-Doxorubicin Complex for Tumor Cell Treatment In Vitro and In Vivo. *J. Biomed. Nanotechnol.* **2015**, *11*, 1139–1152. [CrossRef]
29. Andrievsky, G.; Klochkov, V.; Derevyanchenko, L. Is the C₆₀ Fullerene Molecule Toxic? *Fuller. Nanotub. Carbon Nanostruct.* **2005**, *13*, 363–376. [CrossRef]
30. Prylutska, S.; Bilyy, R.; Overchuk, M.; Bychko, A.; Andreichenko, K.; Stoika, R.; Ritter, U. Water-soluble pristine fullerenes C60 increase the specific conductivity and capacity of lipid model membrane and form the channels in cellular plasma membrane. *J. Biomed. Nanotechnol.* **2012**, *8*, 522–527. [CrossRef]
31. Qiao, R.; Roberts, A.P.; Mount, A.S.; Klaine, S.J.; Ke, P.C. Translocation of C60 and Its Derivatives Across a Lipid Bilayer. *Nano Lett.* **2007**, *7*, 614–619. [CrossRef]
32. TURBOMOLE 7.0. Available online: <http://www.turbomole.com/>.
33. Potemkin, V.; Grishina, M. Principles for 3D/4D QSAR classification of drugs. *Drug. Discov. Today* **2008**, *13*, 952–959. [CrossRef]
34. Potemkin, V.A.; Grishina, M.A. A new paradigm for pattern recognition of drugs. *J. Comput. Aided Mol. Des.* **2008**, *22*, 489–505. [CrossRef]
35. Chemosophia. Available online: <http://www.chemosophia.com/> (accessed on 1 March 2017).
36. Eckert, F.; Klamt, A. Fast solvent screening via quantum chemistry: COSMO-RS approach. *AIChE J.* **2002**, *48*, 369–385. [CrossRef]
37. Trott, O.; Olson, A.J. AutoDock Vina: Improving the speed and accuracy of docking with a new scoring function, efficient optimization, and multithreading. *J. Comput. Chem.* **2010**, *31*, 455–461. [CrossRef]
38. PubChem. Available online: <https://pubchem.ncbi.nlm.nih.gov/> (accessed on 1 May 2019).
39. Bartashevich, E.V.; Potemkin, V.A.; Grishina, M.A.; Belik, A.V. A Method for Multiconformational Modeling of the Three-Dimensional Shape of a Molecule. *J. Struct. Chem.* **2002**, *43*, 1033–1039. [CrossRef]
40. Rosita, G.; Manuel, C.; Franco, M.; Cinzia, N.; Donatella, F.; Emiliano, L.; Roberta, G. Permethrin and its metabolites affect Cu/Zn superoxide conformation: Fluorescence and in silico evidences. *Mol. Biosyst.* **2015**, *11*, 208–217. [CrossRef]
41. Mangiaterra, G.; Laudadio, E.; Cometti, M. Inhibitors of multidrug efflux pumps of *Pseudomonas aeruginosa* from natural sources: An in silico high-throughput virtual screening and in vitro validation. *Med. Chem. Res.* **2017**, *26*, 414–430. [CrossRef]
42. Maier, J.A.; Martinez, C.; Kasavajhala, K.; Wickstrom, L.; Hauser, K.E.; Simmerling, C. ff14SB: Improving the Accuracy of Protein Side Chain and Backbone Parameters from ff99SB. *J. Chem. Theory Comput.* **2015**, *11*, 3696–3713. [CrossRef]
43. Bayly, C.I.; Cieplak, P.; Cornell, W.; Kollman, P.A. A well-behaved electrostatic potential based method using charge restraints for deriving atomic charges: The RESP model. *J. Phys. Chem.* **1993**, *97*, 10269–10280. [CrossRef]
44. Adelman, S.A. Generalized Langevin equation approach for atom/solid-surface scattering: General formulation for classical scattering off harmonic solids. *J. Chem. Phys.* **1976**, *64*, 2375. [CrossRef]
45. Humphrey, W.; Dalke, A.; Schulten, K. VMD: Visual molecular dynamics. *J. Mol. Graph.* **1996**, *14*, 33–38. [CrossRef]

46. Miller, B.R.; McGee, T.D.; Swails, J.M. *MMPBSA.py: An Efficient Program for End-State Free Energy Calculations*. *J. Chem. Theory Comput.* **2012**, *8*, 3314–3321. [[CrossRef](#)]
47. Case, D.A.; Babin, V.; Berryman, J.T.; Betz, R.M.; Cai, Q.; Cerutti, D.S.; Cheatham, T.E., III; Darden, T.A.; Duke, R.E.; Gohlke, H.; et al. *AMBER 14*; University of California: Oakland, CA, USA, 2014.



© 2019 by the author. Licensee MDPI, Basel, Switzerland. This article is an open access article distributed under the terms and conditions of the Creative Commons Attribution (CC BY) license (<http://creativecommons.org/licenses/by/4.0/>).